

Self-Sacrificial Copper Cluster-Catalyzed Oxygen Reduction: A Paradigm Shift in Zinc-Air Battery Technology

Murali Punniyamoorthy, Nadar Allwyn, Kalaivanan Ramamurthy, Murugavel Kathiresan,* and Marappan Sathish*

Metal-ion decorated covalent organic frameworks (M-COFs) are prepared by reacting aldehyde-terminated Cu(I) clustered monomers and amine-terminated triazine monomers through imine linkages, and the as-prepared Cu(I) cluster-based COF is analyzed and tested for its electrocatalytic activity toward oxygen reduction reactions. These M-COFs are more stable and active under adverse conditions. The annealed sample (ACu-COF) displays an increased surface area of $120 \text{ m}^2 \text{ g}^{-1}$ compared to the pristine sample Cu-COF ($19 \text{ m}^2 \text{ g}^{-1}$). Because of its larger specific surface area, and active nitrogen content, the annealed counterpart with flower morphology exhibits exceptional oxygen reduction

reaction (ORR) capabilities. The ACu-COF sample demonstrates a nearly four-electron ORR process, an onset potential of 0.92 V versus reversible hydrogen electrode (RHE), and a diffusion limiting current density of 3.85 mA cm^{-2} . It also reached a half-wave potential of 0.78 V versus RHE. After 2000 cycles, the onset potential of the ACu-COF only dips by 28 mV , demonstrating its remarkable long-term durability. Additionally, the homemade primary zinc-air battery employing ACu-COF produces a specific capacity of 747 mAh g^{-1} and a maximum peak power density of 133 mW cm^{-2} .

1. Introduction

Mankind must create a sustainable, affordable, and renewable alternative to conventional fossil fuels because they are nonrenewable and pollute the environment. These renewable substitutes, in the long term, will have an impact on steady economic growth. Subsequently, it is crucial to the development of energy storage and conversion technologies that are both environmentally friendly and efficient is imperative. Thus, major research is extensively being carried out to find alternate sources of energy^[1–5] which include a variety of energy storage technologies, including lithium-ion,^[6–8] redox flow,^[9,10] and sodium-ion batteries,^[11–13] and their technical advancements. Long used as corporate energy storage devices, lithium-ion batteries (LIBs) have the advantages of high transport of energy efficiency, greater voltage efficiency, and prolonged cycle life. Nonetheless, the mounting concerns around safety, high prices, and a lack of

lithium supplies led the way for alternates such as sodium-ion batteries, metal-air batteries, etc., The most advanced kind of metal-air batteries (MABs), aqueous zinc-air batteries (ZABs), supply the most promise for use in future energy applications compared to Mg-air batteries.^[14–17] A conventional ZAB is composed of an alkaline electrolyte, a zinc anode, and an oxygen-permeable cathode.^[18] Because atmospheric oxygen and zinc are both readily available and are recyclable materials, ZABs are often affordable. However, the oxygen reduction reaction (ORR) is an essential process in these devices that is generally overcome using a noble metal-based electrocatalyst. As noble metals are of high cost and scarce, the development of efficient and high-performing non-noble metal catalysts to speed up the sluggish ORR process is crucial for fuel cell and MABs applications in real-world circumstances.^[19,20]

Recent years have seen a significant increase in research on ORR electrocatalysts due to the increase in demand to find alternate non-noble metal catalysts that are efficient, robust, and exhibit on-par performance with Pt-based catalysts. Among various electrocatalysts, M-N-C-based catalysts M stands for the earth-abundant 3d transition metals (Fe, Co, Ni, Cu, Zn, etc.)^[21–23] are very interesting and the most promising alternatives to precious metal catalysts. For researchers working in reticular chemistry, the M–N–C bond can be formed by fusing molecular building blocks such as covalent organic frameworks (COFs) and metal–organic frameworks (MOFs), with nitrogen-rich core or linker molecules. MOFs frequently confront stability problems because of their coordinate bonds that have significantly lower strengths compared to robust COFs with covalent linkages.^[24] This is particularly true in hostile chemical conditions like boiling water, strong acids, and alkaline environments, and interactions with extremely reactive substrates.^[25] However, COFs could achieve remarkable

M. Punniyamoorthy, N. Allwyn, M. Kathiresan, M. Sathish
Academy of Scientific and Innovative Research (AcSIR)
Ghaziabad 201002, India
E-mail: mkathir.cecri@csir.res.in
msathish.cecri@csir.res.in

M. Punniyamoorthy, K. Ramamurthy, M. Kathiresan
Electro Organic and Materials Electrochemistry Division
CSIR-Central Electrochemical Research Institute (CECRI)
Karaikudi, Tamil Nadu 630003, India

N. Allwyn, M. Sathish
Electrochemical Power Sources Division
CSIR-Central Electrochemical Research Institute (CECRI)
Karaikudi, Tamil Nadu 630003, India

 Supporting information for this article is available on the WWW under <https://doi.org/10.1002/batt.202500588>

stabilities under harsh circumstances with the invention of dynamic covalent chemistry (DCC).^[26–28] Still, the lack of metals hampers the abilities and prospective uses in catalysis. In order it is speculated that “cream-skimming” coordination chemistry and DCC would solve these issues and perhaps introduce hitherto unheard-of levels of structural complexity and functional diversity. M-COFs possess exceptional features such as extremely low density, high porosity, and active metal centers that have garnered notable attention from various fields such as optoelectronics, energy storage, gas separation, storage, etc. High-charge transport mobility is mainly made possible by the extended π -conjugated structure of COFs, which are found both in-plane and between layers.^[28,29] Despite conventional M-N-C catalysts^[30,31] or COF-derived catalysts, which frequently rely on metal salts or postsynthetic doping, our strategy employs “self-sacrificial Cu clusters” embedded within a COF precursor. These clusters work as both a metal supply and a structure-regulating mediator, resulting in uniformly distributed Cu—N—C active sites during annealing. These sites efficiently adsorb and activate O₂ molecules, thereby facilitating a 4-electron ORR route required for high-performance ZABs. The active sites responsible for ORR in our catalyst are Cu—N—C moieties, which are composed of atomically scattered Cu atoms coordinated with nitrogen inside a carbon matrix. After high-temperature annealing, the matrix accumulates pyridinic and graphitic nitrogen species, which improve electrical conductivity and stabilize the Cu—N—C coordination. These sites effectively adsorb and activate O₂ molecules, supporting a 4-electron ORR pathway that is essential for high-performance ZABs.

This work integrates cyclic trinuclear units (CTUs) incorporating d¹⁰ metals with “N” rich triazine units that are prepared step-wise as well as one-pot synthesis under the solvothermal condition. The CTUs group of metal clusters has distinctive features like metallophilic attraction, π -acidity/basicity, luminescent features, and unsaturated metal centers. The metal centers have a low oxidation state, where d¹⁰ metals often have partially occupied 3d orbitals with an appropriate d-band structure, which ensures quick charge transfer during a catalytic process and moderate adsorption/desorption strength.^[32] These systems are still too unstable for practical applications because of their unattractive physical and chemical instability with partially occupied 3d orbitals that participate in Fenton reactions and significantly degrade ionomers. Herein, we report the development of a 2D Cu(I)-triazine interconnected COFs (Cu-COF) via an imine condensation reaction between Cu₃L₃ as the cluster units and an organic linker reaction employing 1, 3, 5-tris-(4-aminophenyl) triazine in a step-wise as well as using a one-pot reaction. In tubular furnaces, Cu-COF is annealed to obtain ACu-COF and as a result, a material with a high porosity and large surface area is produced, enhancing the performance of the 4-electron ORR process, which obtained an onset potential of 0.92 V versus reversible hydrogen electrode (RHE), and diffusion limiting current density of 3.85 mA cm⁻² with exceptional stability and durability. Followed by that, a primary ZAB was designed with ACu-COF, which delivered a maximum peak power density of 133 mW cm⁻² and a specific capacity closer to the theoretical maximum (747 mAh g⁻¹). This study reveals a new M-COF-based electrode material for ZABs, leading the way

for fully exposing numerous active centers of crystalline COFs and boosting their structure and application in the area of energy storage.

2. Experimental Section

2.1. Synthesis of Cu-COF

2.1.1. Stepwise Synthesis of Cu-COF

Cu₃L₃ (23.7 mg, 0.05 mmol) and 4,4', 4-(1,3,5-triazine-2,4,6-triyl) trianiline (26.5 mg, 0.075 mmol) were mixed together in a 10 mL autoclave. The combination has been suspended in 0.5 mL of mesitylene, 0.5 mL of dioxane, and 0.1 mL of 6 M aqueous acetic acid. To remove dissolved oxygen, argon gas was purged for 15 min. The autoclave was heated to 120 °C for 72 h then cooled to ambient temperature. The pale green solid from each tube was isolated by filtration, washed, and solvent exchanged with tetrahydrofuran (THF) and fresh dimethylformamide (DMF). The resultant solids were dried under vacuum at 100 °C for 8 h to give Cu-COF as pale green powders. (**Scheme 1**)

2.1.2. One-Pot Synthesis of Cu-COF

A similar procedure was followed and instead of Cu₃L₃, 1H-pyrazole-4-carbaldehyde, and cupric oxide were used as the source for the preparation of one-pot synthesis of Cu-COF.

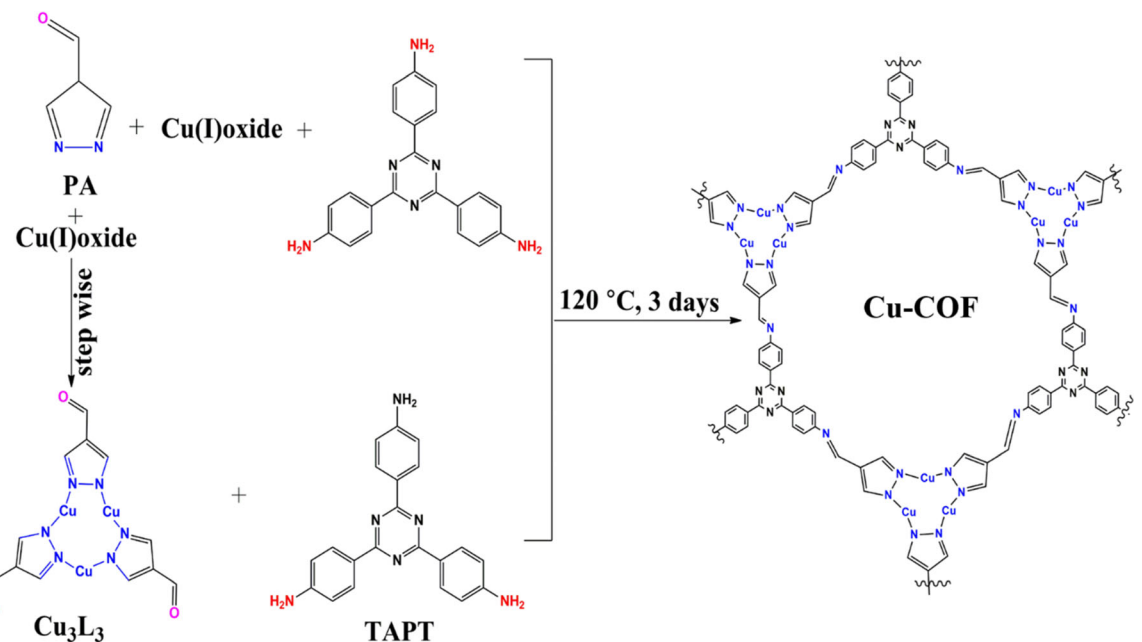
2.1.3. Fabrication of ACu-COF

To activate Cu-COF, the prepared Cu-COF was annealed in a tubular furnace with an argon atmosphere for 2 h at 800 °C.

3. Result And Discussion

3.1. Material Characterizations

The first synthetic effort took place step-by-step, using solvothermal conditions to create discrete, planar Cu₃L₃ single crystals. Cu₃L₃ complexes produced a column packing exhibiting intermolecular Cu…Cu lengths of 3.74 Å, indicating moderate metal-metal interactions, as demonstrated by a single crystallographic study reported by Dan Li et al.^[33] The step-wise process of solvothermolysis produced crystalline products with hexagonal symmetry of hxl lamellar structures of Cu-COF (Figure S1, Supporting Information) by suspending triangular Cu₃L₃ and organic linkers TAPT. At the same time, crystalline Cu-COF can also be made rapidly from a one-pot reaction of the Cu₂O, PY, and TAPT. Individually, previous studies on one-pot synthesis have also noted comparable observations (Figure S2, Supporting Information).^[34,35] The Cu-COF effective transformation is indicated by the elimination of the TAPT-specific N—H stretching vibration band at 3300 cm⁻¹, the aldehydic C—H at



Scheme 1. Step-wise and one-pot synthesis of Cu-COF.

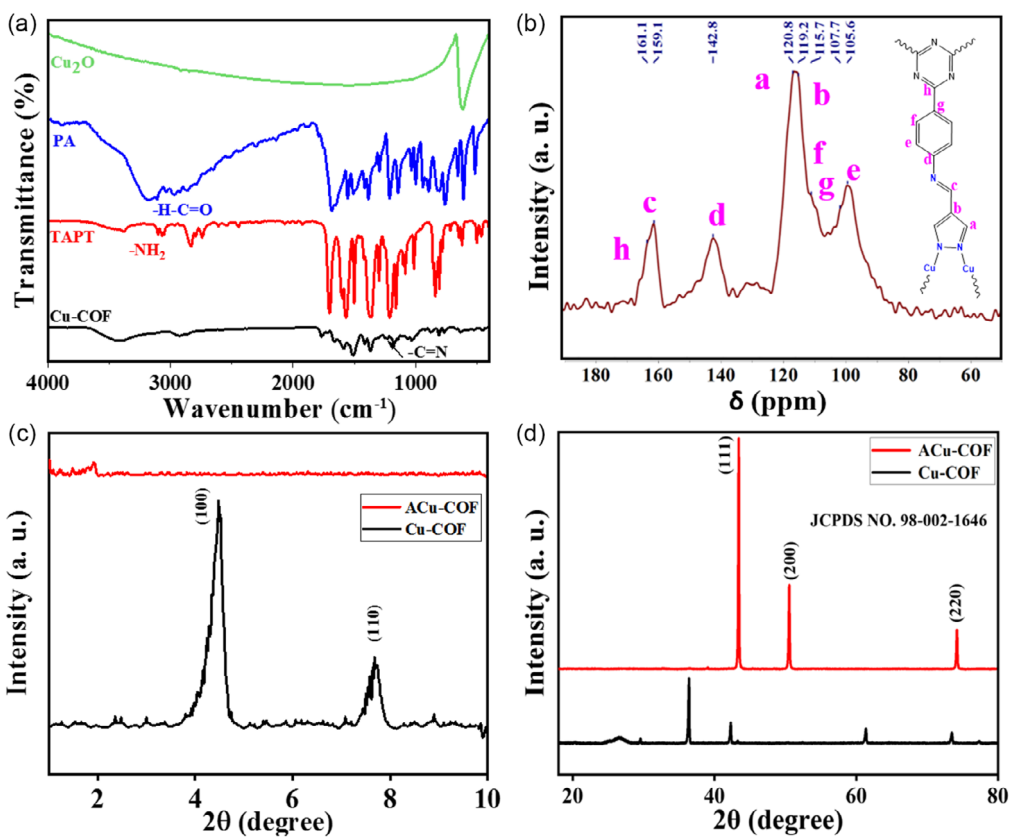


Figure 1. a) FT-IR spectrum of Cu-COF and its precursors, b) ¹³C CP/MAS NMR spectrum of Cu-COF, c,d) low and high angle XRD pattern of Cu-COF and ACu-COF.

2895 cm^{-1} , and the C=O stretching at 1664 cm^{-1} of the aldehyde in the fourier-transform infrared spectroscopy (FT-IR). The -C-N- stretching vibration in Cu-COF is observed as a sharp peak at

1255 cm^{-1} (Figure 1a).^[36] The powder X-ray diffraction (PXRD) arrangement with the (100) plane in Figure S3, Supporting Information ensures the framework's long-range order to adhere

to the crystalline nature of the Cu-COF.^[37] Figure 1b shows the ¹³C CP/MAS NMR signals of Cu-COF. The peaks observed at δ 161, 159, 143, 120, 119, 115, 107, and 105 ppm are attributed to varying kinds of carbon atoms found in the material. The triazine ring's "C" is confirmed by the signal at δ 161 ppm, whereas the pyrazole carbon is responsible for the signal near δ 120 ppm. The presence of the imine group is signified by the peak at δ 143 ppm.^[37,38] Through the use of solid-state NMR and FT-IR spectra, the successful formation of a triazine core and an imine-linked Cu-based COF was confirmed. Thermal gravimetric analysis (TGA) was utilized to determine the thermal stability of COF in a nitrogen environment, as displayed in Figure S4, Supporting Information. The TGA profile indicates that 65.3% of the sample survived thermal treatment at 900 °C. To improve the porosity and electrocatalytic activity of the Cu-COF, it was annealed in a furnace at 800 °C for 2 h. This was done to improve the active catalytic sites in COF, which will result in improved porosity and enhanced electrocatalytic activity.^[39,40] The annealed Cu-COF sample was named as ACu-COF. In the bare Cu-COF, a few traces of copper (I) oxide impurity were unavoidable. The low-angle PXRD patterns confirm that after-annealing, ACu-COF lost the long-range order, and copper has been converted to its corresponding metallic form, which is evident from its corresponding JCPDS pattern (98-002-1446) (Figure 1c,d). The binding energy scale of the X-ray photoelectron spectra (XPS) was calibrated using the C 1s peak at 284.8 eV as a reference, which is a widely used standard in XPS analysis.^[41] To figure out the

oxidation states of Cu in Cu-COF and ACu-COF, the XPS spectra were done for both the samples, and the obtained curve was deconvoluted, as shown in Figure 2a, which showed two peaks. The spin-orbit coupling of 2p electrons creates two different peaks, corresponding to $2p_{3/2}$ and $2p_{1/2}$ at 932.71 and 952.71 eV, respectively.^[33,42] These peaks indicate that Cu is in +1 oxidation state for Cu-COF. But in the case of ACu-COF, due to the formation of a trace amount of oxide over the surface of metallic copper, weak peaks characteristic of oxidized copper was evident. Two peaks at 400.2 and 402 eV can be observed in the N 1s spectrum of Cu-COF (Figure 2b) which represents the imine and triazine nitrogen, whereas in the N 1s spectrum of ACu-COF in addition to imine and triazine N, it exhibits pyridinic and graphitic nitrogen, respectively (Figure 2c). The presence of pyrrolic, pyridinic, and graphitic nitrogen is equally important for ORR catalytic activity. Graphitic nitrogen may be produced by annealing at 800 °C in an argon atmosphere.^[43] The degree of porosity in terms of size and distribution was calculated using nitrogen adsorption and desorption isotherms. Materials with a high specific surface area, as well as mesopores and micropores, facilitate proton and electron transport throughout the ORR mechanism. The ACu-COF had a significantly larger specific surface area of $120 \text{ m}^2 \text{ g}^{-1}$ than its unannealed counterpart, Cu-COF, which exhibited a specific surface area of $19 \text{ m}^2 \text{ g}^{-1}$ (Figure 2d), indicating that the annealed one had a greater porosity with a large number of exposed active sites. The increased catalytic surface area of the annealed one promotes faster

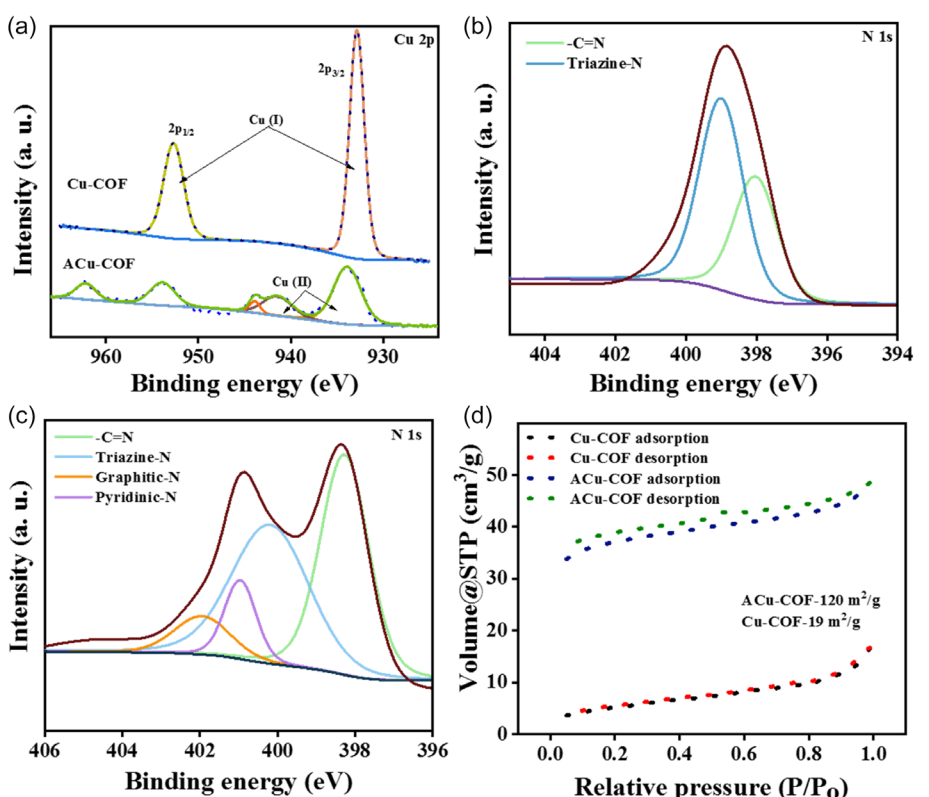


Figure 2. a) Cu 2p high-resolution XPS spectrum of Cu-COF and ACu-COF, b) N 1s spectrum of Cu-COF, c) N 1s spectrum of ACu-COF, and d) Nitrogen adsorption-desorption isotherms of Cu-COF and ACu-COF.

charge transfer for the ORR process. The field emission scanning electron microscope (FE-SEM) shows that the morphology is retained in ACu-COF and Cu-COF even after 800 °C annealing. **Figure 3a,f** clearly show that both contain flower-like morphology.^[44] The HR-TEM picture shown in Figure 3b-d and g-h at three magnification scales demonstrates the existence of a flower-like morphology of Cu-COF and ACu-COF. Figure 3e,i demonstrates the selected area electron diffraction pattern, which confirms the polycrystalline nature of the Cu-COF and ACuCOF.^[45] The elemental mapping images reveal that Cu in Cu-COF and ACu-COF was distributed consistently across the framework (Figure S5, Supporting Information). According to the FE-SEM energy dispersive X-ray analysis (EDX) measurements, the weight contents of Cu in Cu-COF were 27 wt%, and in ACu-COF was 19 wt% (Figure S6 and S7, Supporting Information). The ORR activity generally reaches its peak due to the large amount of nitrogen present in the form of pyridinic and graphitic species in the structure. The pyridinic and graphitic nature of nitrogen suggests greater exposure of the outermost plane, which enhances oxygen diffusion and adsorption, thereby weakening the O—O bond.

Extensive studies on the material show that ACu-COF possesses a large surface area with evenly distributed nitrogen and copper, making it ideal for ORRs and ZABs. To obtain more information on the electrochemical behavior of these synthesized materials, electrocatalytic oxygen reduction was conducted systematically.

3.2. Electrochemical Oxygen Reduction Reaction Performance

Cyclic voltammetry was applied to determine the oxygen reduction capacities of Pt/C (20%), ACu-COF, and Cu-COF in 0.1 M KOH solution under nitrogen and oxygen-saturated conditions. **Figure 4a** illustrates a strong, significant cathodic reduction peak for Pt/C at 0.74 V, ACu-COF at 0.67 V, and Cu-COF appeared at 0.47 V versus RHE in oxygen-saturated conditions, which is missing in N₂-saturated environments (Figure S8, Supporting Information). ACu-COF and Cu-COF achieved an onset potential of 0.92 and 0.75 V versus RHE, demonstrating that ACu-COF is more ORR active and comparable to the benchmark catalyst, Pt/C (1.05 V against RHE). This shows that both systems may undergo an oxygen reduction process (Figure 4b). The obtained

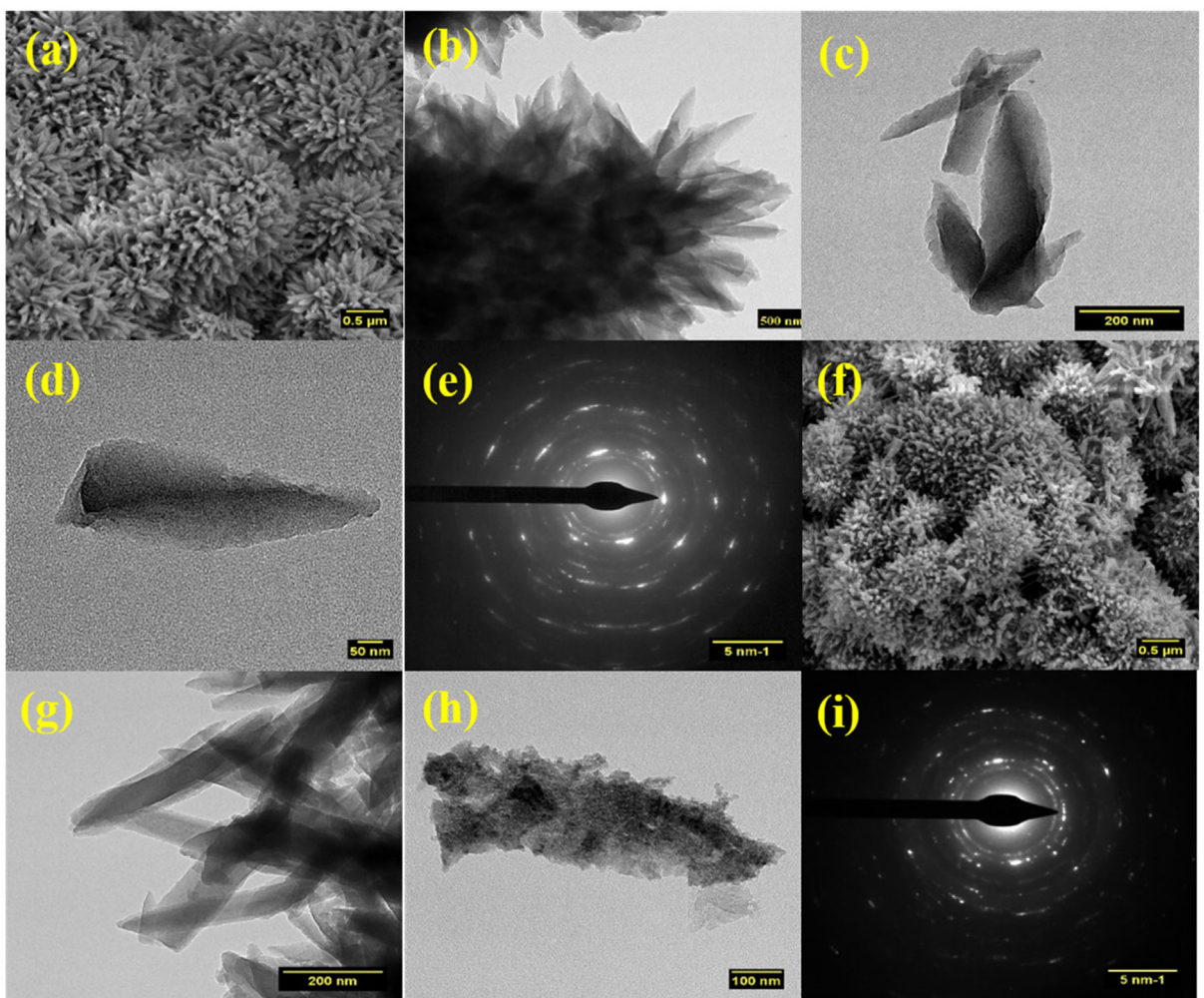


Figure 3. a) FE-SEM image of Cu-COF, b-d) HR-TEM images of Cu-COF, e) SAED pattern of Cu-COF, f) FE-SEM image of ACu-COF, and g-i) HR-TEM images of ACu-COF at different magnifications.

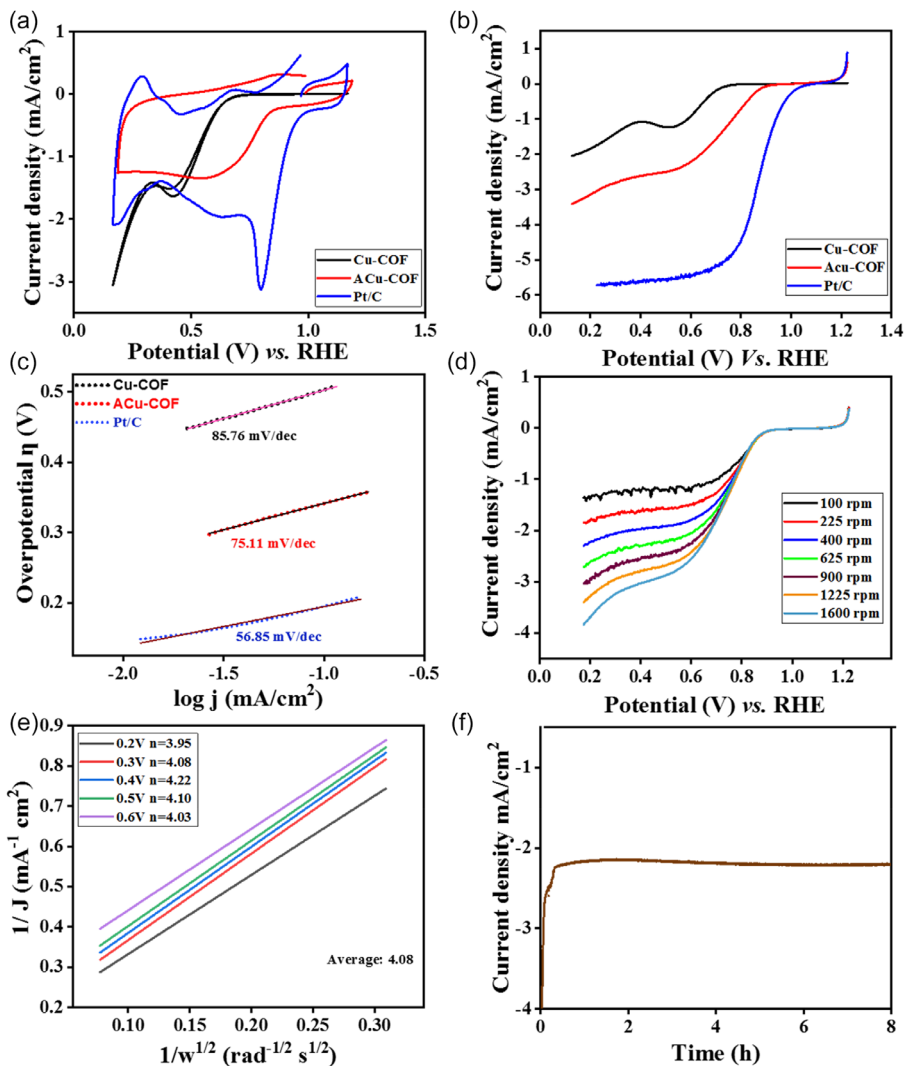


Figure 4. a) Cyclic voltammogram of Cu-COF, ACu-COF, and Pt/C (20%) in 0.1 M KOH in an O₂ atmosphere. b) LSV comparison plot of ACu-COF with Cu-COF and Pt/C in 0.1 M KOH at 1600 rpm. c) Tafel plot with the corresponding Tafel slope value for ACu-COF, Cu-COF, and 20% Pt/C d) LSV plot of ACu-COF at various rpm in 0.1 M KOH at the scan rate of 5 mV s⁻¹. e) Koutecky-Levich plot of ACu-COF and the number of electrons transferred. f) Chronoamperometry study in oxygen-saturated 0.1 M KOH.

half-wave potential ($E_{1/2}$) and limiting current density (j_d) from linear sweep voltammetry (LSV) for ACu-COF were 0.78 V and 3.85 mA cm⁻², respectively; however, the $E_{1/2}$ and j_d values for Cu-COF were 0.64 V and 1.78 mA cm⁻², indicating that ACu-COF exhibited much higher ORR activity at 1600 rpm at a scan rate of 5 mV s⁻¹. ACu-COF had a 310 mV dip in overpotential compared to the theoretical value (1.23 V), similarly, its half-wave potential was closer to the benchmark Pt/C. Tafel slope is a crucial kinetic measurement for understanding the kinetics of the transport of electrons. The Tafel plot in Figure 4c demonstrates ACu-COF's superior performance against ORR, as it has the lowest Tafel slope value compared to the unannealed Cu-COF catalyst. The decrease in the Tafel slope of 75.1 mV dec⁻¹ for ACu-COF compared to 85.7 mV dec⁻¹ for Cu-COF suggests a faster electron transfer reaction in ACu-COF material. The pristine Cu-COF demonstrated low ORR activity, which could be attributed to low porosity caused by the presence of heavier solvent molecules

with poor electrical conductivity. The ORR activity was further investigated by undertaking LSV in an oxygen-saturated 0.1 M KOH solution in an RDE setup rotating at a rate ranging from 100 to 1600 rpm (Figure 4d). Furthermore, the Koutecký-Levich (KL) plot showed outstanding linearity at varied potential, indicating that all molecules of oxygen undergo reduction with the same number of electrons, pursuing a single process (Figure 4e).^[46,47] The electron-transfer number of ACu-COF was found to be 4.08, nearly comparable to that of Pt/C ($n = 4.2$), indicating a quicker kinetics ORR. The accelerated degradation study was performed by doing 2000 cycles of cyclic voltammetry at a scan rate of 100 mV s⁻¹ and a potential range of 0.2–1.2 V vs. RHE, and then performing by running LSV at 1600 rpm in the identical potential window (Figure S9, Supporting Information). The collected information shows that just 28 mV of E_{onset} deteriorated after 2000 cycles, indicating the high durability of the catalyst (ACu-COF). The stability of the ACu-COF catalyst was further

evaluated through the chronoamperometry technique, as shown in Figure 4f, demonstrating its remarkable durability over 8 h. Furthermore, the electrochemical active surface area (ECSA) measurement revealed that ACu-COF required a higher double-layer capacitance (C_{dl}) of $85 \mu\text{F cm}^{-2}$, compared to Cu-COF's capacitance of $8 \mu\text{F cm}^{-2}$ (Figure S10, Supporting Information). As the C_{dl} value rises, it implies that ECSA is larger and that more active sites will be exploited in ACu-COF than in Cu-COF. The catalytic activity may be attributed to the following reasons. The Cu—N—C moieties, covalently anchored on electronically conductive substrates, represent a promising strategy for efficient ORR catalysis. The self-sacrificial Cu clusters embedded within the COF precursor serve as an ideal catalytic center for the four-electron ORR pathway. The strong Cu—N—C coordination enhances O—O bond activation and optimizes the adsorption energies of O_2 and $-\text{OOH}^*$ intermediates, thereby improving the thermodynamics and overall catalytic activity of the Cu—N—C sites.^[48]

3.3. Investigating the Electrochemical Behavior of Zinc-Air Batteries

The exceptional ORR activity, kinetics, and stability of ACu-COF made it an ideal oxygen electrode in a primary ZAB. The battery's configuration consisted of a gas diffusion layer a coated with

ACu-COF catalyst as the air-permeable cathode, a zinc sheet as the anode, and 6 M KOH with 0.25 M zinc acetate mixture as the electrolyte.^[49] The ACu-COF-based battery displayed an open-circuit voltage of 1.436 V (Figure 5a). Over 10 h, the device maintained a stable OCV plateau without voltage decay. Figure 5b displays the polarization and power density curves for both ACu-COF and Pt/C. The ACu-COF device showed a higher current density of 60 mA cm^{-2} at 1 V, surpassing Pt/C by 10 mA cm^{-2} . Though both ACu-COF and Pt/C displayed almost similar profiles in the low current density region, the plot of the former was comparatively flatter and more stable in the high current density region praising its exceptional stability in the highly alkaline battery condition and high current density. Notably, as an outcome of the above, the ACu-COF-based ZAB achieved a peak power density of 133 mW cm^{-2} at 300 mA cm^{-2} , significantly higher than the commercial cathode's 125 mW cm^{-2} . Rate capability tests (Figure 5c) demonstrated minimal voltage drop with increasing current density. The device was susceptible to a maximum current density of 30 mA cm^{-2} but suffered slight instability after that, which is evident from the corresponding profile. After discharging at 50 mA cm^{-2} , the battery retained 99.8% of its voltage when again discharged at 5 mA cm^{-2} . Long-term discharge at 5 mA cm^{-2} showed remarkable stability, maintaining 1.19 V with

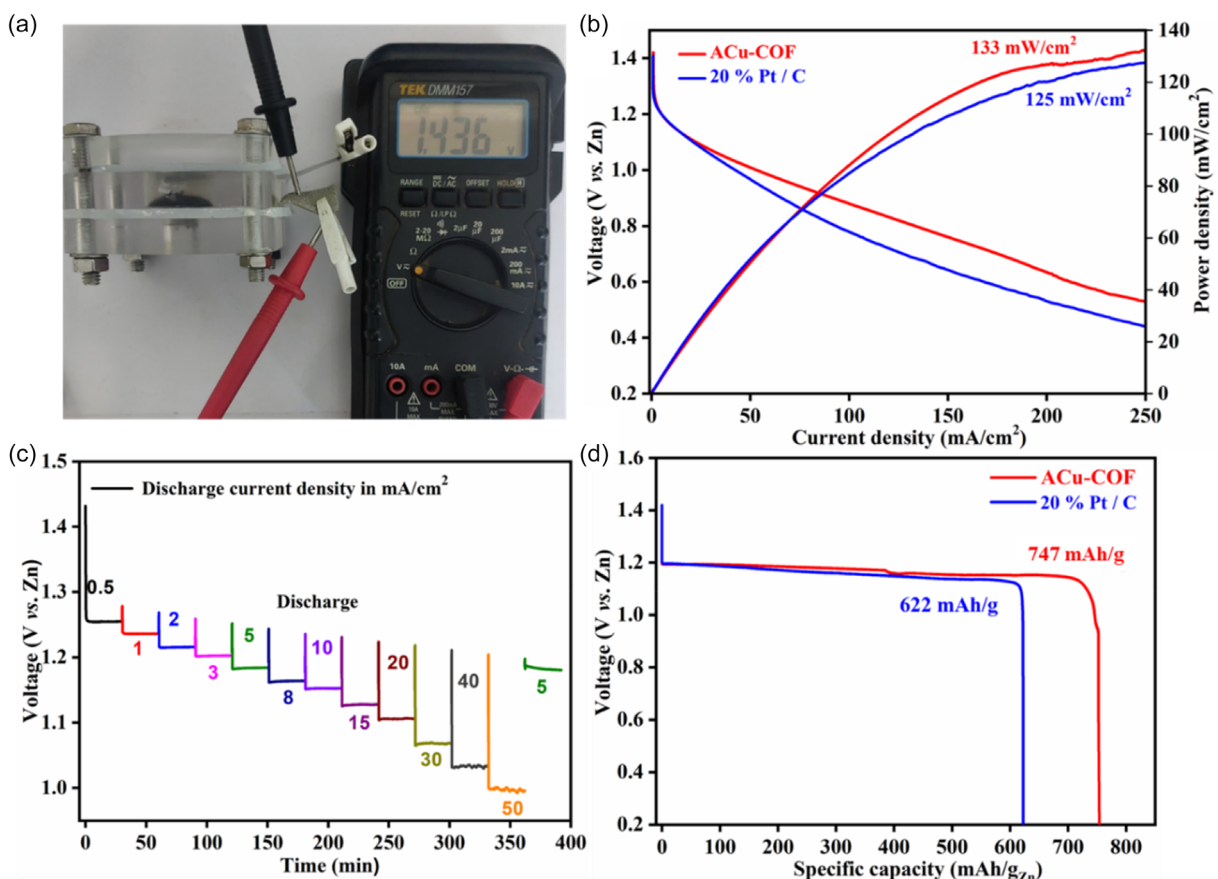


Figure 5. a) OCV of assembled ACu-COF electrocatalyst based primary zinc-air battery, b) polarization cum power density profile of ACu-COF and Pt/C based primary zinc-air battery, c) rate capability plot of ACu-COF based primary zinc-air battery at various current densities from 0.5 to 50 mA cm^{-2} and again to 5 mA cm^{-2} , and d) specific capacity plot of ACu-COF and Pt/C based primary zinc-air battery by completely deep discharging the device.

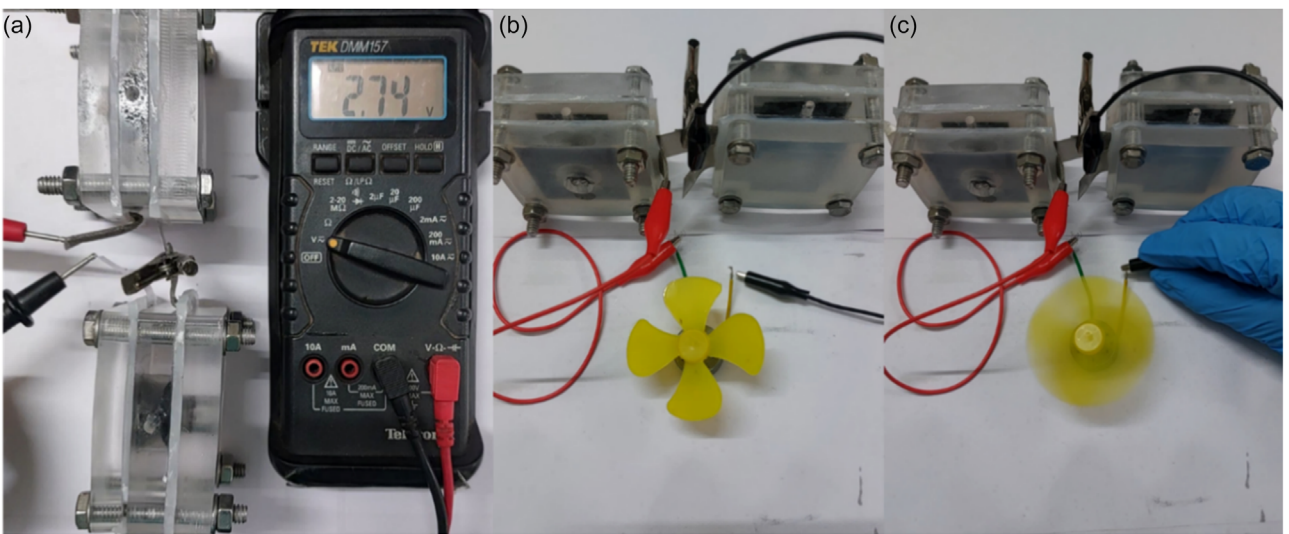


Figure 6. a) OCV of series assembled ACu-COF based primary zinc-air battery, and b,c) ACu-COF based primary zinc-air battery powering a motor-based toy fan.

negligible activity decay even after 30 h. The ACu-COF-based battery's specific capacities reached 90% of the theoretical values (747 mAh g^{-1}), which was higher than the corresponding Pt/C (622 mAh g^{-1}), underscoring its exceptional performance (Figure 5d). Table S1, Supporting Information shows the performance comparison of ACu-COF based ZAB with recent literature. Connecting two ZABs in series yielded an impressive overall open-circuit voltage of 2.74 V (Figure 6a) which was sufficient to power up a motorized toy fan for over 5 h continuously (Figure 6b-c). These demonstrations showcase the exceptional discharge performance and rate capability of ACu-COF as an ORR catalyst in ZABs, confirming its viability for practical applications.

4. Conclusion

We have demonstrated a process for the preparation of "N" rich triazine moiety interconnected cyclic trinuclear units (CTUs) integrating d¹⁰ metals employing a Schiff base condensation method via one-pot as well as step-wise approach under solvothermal conditions. Further, to improve the porosity and electrocatalytic activity of Cu-COF, the as-prepared material was annealed in a tubular furnace at 800 °C. As a result, annealed ACu-COF was obtained with high porosity and a wide surface area was formed, and the annealed sample showed excellent electrochemical characteristics than the pristine sample. ACu-COF exhibited excellent electrocatalytic activity for ORR with an onset potential of 0.92 V and a limiting current density of 3.85 mA cm^{-2} , which is similar to the benchmark catalyst Pt/C. Following this, it demonstrated remarkable stability even after conducting a degradation test for 2000 cycles. The ACu-COF-based ZAB showed remarkable performance in terms of having a flat discharge profile with high-rate capability and a maximum peak power density of 133 mW cm^{-2} .

Thus, our work opens a new pathway for the design of an M-COF-based oxygen electrocatalyst for a ZAB.

Acknowledgements

The authors wish to acknowledge Dr. K. Ramesha, Director, CSIR-CECRI for his constant support and encouragement. The Central Instrumentation Facility (CIF) Division of CSIR-CECRI is acknowledged for the characterization facilities. M.P. and N.A. wish to acknowledge UGC for Fellowship. The manuscript communication number is CECRI/PESVC/Pubs./2025–047.

Conflict of Interest

The authors declare no conflict of interest.

Author Contributions

Murali Punniyamoorthy: conceptualization (lead); formal analysis (lead); investigation (lead); methodology (lead); writing—original draft (lead). **Nadar Allwyn:** conceptualization (supporting); formal analysis (equal); methodology (supporting); writing—original draft (equal). **Kalaivanan Ramamurthy:** data curation (supporting); investigation (supporting); software (supporting); validation (supporting). **Murugavel Kathiresan:** conceptualization (lead); investigation (lead); methodology (lead); project administration (lead); supervision (lead); writing—review & editing (lead). **Marappan Sathish:** conceptualization (lead); formal analysis (lead); validation (lead); writing—review & editing (lead).

Data Availability Statement

The data that support the findings of this study are available from the corresponding author upon reasonable request.

Keywords: imine linkage · metal covalent organic framework · oxygen reduction reactions · triazine · zinc-air batteries

- [1] M. M. Rahman, A. O. Oni, E. Gemedu, A. Kumar, *Energy Convers. Manage.* **2020**, *223*, 113295.
- [2] L. Trahey, F. R. Brushett, N. P. Balsara, G. Ceder, L. Cheng, Y. M. Chiang, N. T. Hahn, B. J. Ingram, S. D. Minteer, J. S. Moore, K. T. Mueller, L. F. Nazar, K. A. Persson, D. J. Siegel, K. Xu, K. R. Zavadil, V. Srinivasan, G. W. Crabtree, *Proc. Natl. Acad. Sci. U.S.A.* **2020**, *117*, 12550.
- [3] J. B. Goodenough, *Energy Storage Mater.* **2015**, *1*, 158.
- [4] Y. Yan, J. Lin, K. Huang, X. Zheng, L. Qiao, S. Liu, J. Cao, S. C. Jun, Y. Yamauchi, J. Qi, *J. Am. Chem. Soc.* **2023**, *145*, 24218.
- [5] S. Liu, L. Kang, J. Hu, E. Jung, J. Zhang, S. C. Jun, Y. Yamauchi, *ACS Energy Lett.* **2021**, *6*, 3011.
- [6] M. Li, J. Lu, Z. Chen, K. Amine, *Adv. Mater.* **2018**, *30*, 1800561.
- [7] A. Manthiram, *ACS Cent. Sci.* **2017**, *3*, 1063.
- [8] A. Väyrynen, J. Salminen, *J. Chem. Thermodyn.* **2012**, *46*, 80.
- [9] P. Vanýsek, V. Novák, *J. Energy Storage* **2017**, *13*, 435.
- [10] E. Ventosa, *Curr. Opin. Chem. Eng.* **2022**, *37*, 100834.
- [11] C. Vaalma, D. Buchholz, M. Weil, S. Passerini, *Nat. Rev. Mater.* **2018**, *3*, 1.
- [12] K. Chayambuka, G. Mulder, D. L. Danilov, P. H. L. Notten, *Adv. Energy Mater.* **2018**, *8*, 1800079.
- [13] P. K. Nayak, L. Yang, W. Brehm, P. Adelhelm, *Angew. Chem., Int. Ed.* **2018**, *57*, 102.
- [14] J. Zhang, Q. Zhou, Y. Tang, L. Zhang, Y. Li, *Chem. Sci.* **2019**, *10*, 8924.
- [15] W. Sun, F. Wang, B. Zhang, M. Zhang, V. Küpers, X. Ji, C. Theile, P. Bieker, K. Xu, C. Wang, M. Winter, *Science* **2021**, *371*, 46.
- [16] J. N. Liu, C. X. Zhao, J. Wang, D. Ren, B. Q. Li, Q. Zhang, *Energy Environ. Sci.* **2022**, *15*, 4542.
- [17] J. Liu, H. Hu, T. Wu, J. Chen, X. Yang, N. Wang, Z. Shi, *J. Magnesium Alloys* **2024**, *12*, 1554.
- [18] X. Zhong, Y. Shao, B. Chen, C. Li, J. Sheng, X. Xiao, B. Xu, J. Li, H.-M. Cheng, G. Zhou, *Adv. Mater.* **2023**, *35*, 2301952.
- [19] Z. Wang, H. Jin, T. Meng, K. Liao, W. Meng, J. Yang, D. He, Y. Xiong, S. Mu, *Adv. Funct. Mater.* **2018**, *28*, 1802596.
- [20] N. Allwyn, B. Ambrose, M. Kathiresan, M. Sathish, *ACS Appl. Energy Mater.* **2023**, *6*, 11408.
- [21] Z. Zhu, J. Cui, X. Cao, L. Yang, H. Sun, W. Liang, J. Li, A. Li, *Int. J. Hydrogen Energy* **2022**, *47*, 9504.
- [22] G.-L. Li, Z.-F. Lu, X. Wang, S. Cao, C. Hao, *ACS Sustainable Chem. Eng.* **2022**, *10*, 224.
- [23] J. Chen, T. Zhou, C. He, Z. Luo, C. Shi, L. Zhang, Q. Zhang, C. He, X. Ren, *Nanoscale* **2024**, *16*, 21515.
- [24] P. Kumar, B. Anand, Y. F. Tsang, K.-H. Kim, S. Khullar, B. Wang, *Environ. Res.* **2019**, *176*, 108488.
- [25] B. Ambrose, R. Madhu, K. Ramamurthy, M. Kathiresan, S. Kundu, *Small* **2024**, *20*, 2402403.
- [26] Y. Deng, Y. Wang, J. Wang, Z. Wei, C. Xin, J. Liu, C. Zhao, Z. Zhang, *Mater. Today Chem.* **2022**, *26*, 101027.
- [27] Z. Lei, H. Chen, S. Huang, L. J. Wayment, Q. Xu, W. Zhang, *Chem. Rev.* **2024**, *124*, 7829.
- [28] J. Hu, S. K. Gupta, J. Ozdemir, H. Beyzavi, *ACS Appl. Nano Mater.* **2020**, *3*, 6239.
- [29] X. Li, K. Kawai, M. Fujitsuka, Y. Osakada, *Surf. Interfaces* **2021**, *25*, 101249.
- [30] K. Huang, Y. Yan, Y. Yu, T. Yang, L. Qiao, J. Tu, J. Sui, W. Cai, S. Liu, X. Zheng, *EES Catal.* **2025**, *3*, 1044.
- [31] W. Zhang, B. Feng, L. Huang, Y. Liang, J. Chen, X. Li, Z. Shi, N. Wang, *Appl. Catal., B* **2024**, *358*, 124450.
- [32] S. Guria, D. Dolui, C. Das, S. Ghorai, V. Vishal, D. Maiti, G. K. Lahiri, A. Dutta, *Nat. Commun.* **2023**, *14*, 6859.
- [33] R. J. Wei, H. G. Zhou, Z. Y. Zhang, G. H. Ning, D. Li, *CCS Chem.* **2021**, *3*, 2045.
- [34] T. Wang, Y.-C. Zhao, M. Luo, L.-M. Zhang, Y. Cui, C.-S. Zhang, B.-H. Han, *Polymer* **2015**, *60*, 26.
- [35] C. Liu, M. Xia, M. Zhang, K. Yuan, F. Hu, G. Yu, X. Jian, *Polymer* **2020**, *194*, 122401.
- [36] R. Gomes, A. Bhaumik, *RSC Adv.* **2016**, *6*, 28047.
- [37] C. Liu, Y. Xiao, Q. Yang, Y. Wang, R. Lu, Y. Chen, C. Wang, H. Yan, *Appl. Surf. Sci.* **2021**, *537*, 148082.
- [38] M. Punniyamoorthy, S. S. Roy, M. Kathiresan, S. Kundu, *ACS Appl. Energy Mater.* **2024**, *7*, 4111.
- [39] Q. Xu, Y. Tang, L. Zhai, Q. Chen, D. Jiang, *Chem. Commun.* **2017**, *53*, 11690.
- [40] R.-J. Wei, H.-G. Zhou, Z.-Y. Zhang, G.-H. Ning, D. Li, *CCS Chem.* **2021**, *3*, 2045.
- [41] T. Yang, Y. Yan, R. Liu, K. Huang, R. Xu, J. Chen, J. Tu, S. Liu, L. Kang, Z. Wang, J. Cao, J. Qi, *Nano Lett.* **2025**, *25*, 7707.
- [42] J.-M. Huang, J. Guo, C. Xu, A. Su, K.-J. Wu, C.-H. He, *Processes* **2024**, *12*, 1520.
- [43] Y. Zhuang, J. Yang, L. Meng, C. Ma, L. Peng, D. Chen, Q. Chen, *Ind. Chem. Mater.* **2023**, *1*, 458.
- [44] Y. He, N. An, C. Meng, K. Xie, X. Wang, X. Dong, D. Sun, Y. Yang, Z. Hu, *J. Mater. Chem. A* **2022**, *10*, 11030.
- [45] S. Bi, C. Yang, W. Zhang, J. Xu, L. Liu, D. Wu, X. Wang, Y. Han, Q. Liang, F. Zhang, *Nat. Commun.* **2019**, *10*, 1930.
- [46] R. Zhou, Y. Zheng, M. Jaroniec, S.-Z. Qiao, *ACS Catal.* **2016**, *6*, 4720.
- [47] S. Xu, Y. Kim, D. Higgins, M. Yusuf, T. F. Jaramillo, F. B. Prinz, *Electrochim. Acta* **2017**, *255*, 99.
- [48] H. Liu, Y. Zhou, S. Zhu, L. Zheng, Z. Cui, Z. Li, S. Wu, L. Ma, Y. Liang, *J. Alloys Compd.* **2021**, *857*, 158321.
- [49] M. Hilder, B. Winther-Jensen, N. B. Clark, *J. Power Sources* **2009**, *194*, 1135.

Manuscript received: August 5, 2025

Revised manuscript received: October 28, 2025

Version of record online: